A Preprint
from the

OWENS VALLEY RADIO OBSERVATORY

California Institute of Technology
Pasadena, California

1972

3. A MODEL OF THE CRAB NEBULA DERIVED FROM DUAL-FREQUENCY RADIO MEASUREMENTS

by
K. W. Weiler and G. A. Seielstad

Security Classification

DOCUMENT CONTROL DATA - R & D

(Security classification of title, body of abstract and indexing annotation must be entered when the overall report is classified)

1. ORIGINATING ACTIVITY (Corporate author)
California Institute of Technology
Owens Valley Radio Observatory
Pasadena, California 91109

2a. REPORT SECURITY CLASSIFICATION
UNCLASSIFIED

2b. GROUP

3. REPORT TITLE
A MODEL OF THE CRAB NEBULA DERIVED FROM DUAL-FREQUENCY RADIO MEASUREMENTS.

4. DESCRIPTIVE NOTES (Type of report and inclusive dates)

5. AUTHOR(S) (First name, middle initial, last name)
K. W. Weiler and G. A. Seielstad

6. REPORT DATE
#3, 1972

7a. TOTAL NO. OF PAGES
28

7b. NO. OF REFS
26

8a. CONTRACT OR GRANT NO
Nonr N00014-67-A-0094-0019

b. PROJECT NO.

c.

d.

9a. ORIGINATOR'S REPORT NUMBER(S)
#3, 1972

9b. OTHER REPORT NO(S) (Any other numbers that may be assigned this report)

10. DISTRIBUTION STATEMENT
This document has been approved for public release and sale; its distribution is unlimited.

11. SUPPLEMENTARY NOTES

12. SPONSORING MILITARY ACTIVITY
Office of Naval Research

13. ABSTRACT

The total intensity and linearly polarized emission from the Crab Nebula (Taurus A) were synthesized to a resolution of approximately 1 arc-minute at both 1420 and 2880 MHz. From these data were calculated the spectral index, rotation measure, intrinsic position angle, and depolarization ratio distributions. Then, combined with a source model, the physical conditions within the supernova remnant were established. The strength and orientation of both the homogeneous and random components of the magnetic field were determined and a measurement of the thermal electron plasma distribution obtained.

I

DD FORM 1 NOV 68 1473

Security Classification

ABSTRACT

The total intensity and linearly polarized emission from the Crab Nebula (Taurus A) were synthesized to a resolution of approximately 1 arc-minute at both 1420 and 2880 MHz. From these data were calculated the spectral index, rotation measure, intrinsic position angle, and depolarization ratio distributions. Then, combined with a source model, the physical conditions within the supernova remnant were established. The strength and orientation of both the homogeneous and random components of the magnetic field were determined and a measurement of the thermal electron plasma distribution obtained.

Address of Authors: Dr. K. W. Weiler
Radiosterrenwacht Westerbork
Post Hooghalen, Netherlands

Dr. G. A. Seielstad
Owens Valley Radio Observatory
California Institute of Technology
P.O. Box 387
Big Pine, California 93513
U.S.A.

Key Words: Supernova, Crab Nebula, Taurus A

I. INTRODUCTION

Earth rotation synthesis observations of the total and linearly polarized radiation from Taurus A (The Crab Nebula) were taken concurrently with those of the two supernova remnants 3C10 (Tycho's Supernova) and 3C58 (Weiler and Seielstad 1971, hereafter referred to as Paper I). The Owens Valley Radio Observatory's interferometer was used at frequencies of both 1420 and 2880 MHz at multiple spacings East-West and North-South and over all hour angles available to the telescopes (-4^h to $+4^h$). The resulting coverage in the Fourier transform (u, v) plane is illustrated in Fig. 1.

The observing methods, dates of observation, and calibration procedure are fully described in Paper I. Briefly, the observations were done by alternating the receiving horns between three different configurations of orthogonal position angles to obtain measures of the Fourier components of the Stokes parameters I+Q, U-iV, and -Q-iV. Since we previously measured an upper limit of 0.2 per cent to the integrated degree of circular polarization of Taurus A at 1418 MHz (Seielstad and Weiler 1968)[1], we assumed that there was no circularly polarized radiation, i.e., V=0.

These three uncorrected sets of data were then inverted into the real plane. However, because of the large gaps evident in

---

[1] G. L. Berge and G. A. Seielstad (unpublished) have measured an upper limit of 0.2 per cent at 1602 MHz also.

Fig. 1 in the information coverage of the Fourier plane, the inversion technique employed in Paper I was no longer appropriate. Instead, we used an inversion scheme developed by J. A. Högbom and described by Rogstad and Shostak (1971). Finally the instrumental corrections (< 0.3 per cent at 1420 MHz and < 0.4 per cent at 2880 MHz) were applied and the solutions combined to yield the distributions of the total radiation (Stokes parameter I), of the linearly polarized radiation ($\sqrt{Q^2+U^2}$), and of the position angles of the maximum electric vectors ($\frac{1}{2}\tan^{-1}(U/Q)$).

II. SOURCE DISTRIBUTIONS

The resulting synthesized maps are displayed in Figs. 2 and 3. All details of position and scale are identical among the several diagrams. The origin is

$$\alpha\ (1950.0) = 05^h\ 31^m\ 31\overset{s}{.}20,$$

$$\delta\ (1950.0) = +21°\ 59'\ 17\overset{''}{.}0$$

Relative to the Sp of the central double stars, this position is $0\overset{s}{.}26$ earlier and $22\overset{''}{.}2$ north. The error analysis and the effects of ionospheric Faraday rotation are discussed in Paper I. The error estimates for the three fundamental maps (I, Q, U) are collected in Table 1.

A. Distributions of the Total Radiation

The brightness distributions of the total radiation at the two frequencies show the same smooth appearance already noted by several previous studies with comparable resolution (Branson

1967; Mayer and Hollinger 1968; Braun and Yen 1968; Johnston and Hobbs 1969; Wright 1970). Only the maps with resolution better by an order of magnitude (Hogg et al. 1969; Wilson 1971) begin to reveal further structural detail. It seems worthwhile repeating that the most remarkable feature of the brightness distribution is its central concentration. Milne (1971) has demonstrated that it is much more common for supernova remnants to show at least partial shell structure.

Wright (1970) has called attention to an extended low brightness region SW of the nebula. There is little evidence for such a feature in either the total or polarized radiation maps. Also, recent λ21 cm maps made with the Westerbork Telescope fail to show such a region (R. M. Duin 1972, private communication).

B. Distributions of Linearly Polarized Radiation

Both distributions of linearly polarized radiation reveal similar structure, which is more detailed than that of the total radiation. There is a conspicuous gap in the NW which is near the most prominent "bay" in the optical distribution (Woltjer 1957). The rapid change of position angles in that region implies that the low radio polarization may result partly from beam-averaging vectors having a wide range of position angles. Higher resolution studies (Conway 1971) confirm this. We find it somewhat surprising that our polarization distributions do not exhibit similar gaps elsewhere, since other prominent

optical bays are known to exist. The center of the polarization distribution in both cases is displaced about 0!25 east and 0!3 south from the center of the total brightness distribution. Other observers (Mayer and Hollinger 1968; Downs and Thompson 1968; Johnston and Hobbs 1969; Wright 1970), confirm most of these features over a wide range of frequencies.

The degree of polarization reaches nearly 4 per cent at 1420 MHz and nearly 8 per cent at 2880 MHz. In both cases it is relatively constant over the main body of the nebula increasing slightly at 21 cm around the disturbed region in the NW. The position angles likewise show a constancy within the main body with a sharp rotation of angles occurring in the NW.

III. PARAMETER DISTRIBUTIONS

Since we have observations at two very different frequencies with the same resolution and with approximately the same Fourier plane coverage, processed in an identical manner, determinations of frequency-dependent parameter distributions are especially reliable. For these distributions we have chosen a coordinate system oriented along the major and minor axes of the source.

A. Spectral Index Distribution

The spatial distribution of spectral indices for Taurus A (defined as $I_\nu \sim \nu^{+\alpha}$) between 1420 and 2880 MHz is presented in Table 2. The spectrum is flattest near the center and steepens progressively along any radial direction outward. This steepening

of spectral index toward the periphery of the nebula was noted between 404 and 1420 MHz also (Davies et al. 1966). Furthermore, Davies et al. (1966) and Scargle (1969) have emphasized that the optical nebula is smaller than the radio, and that the X-ray nebula is smaller yet. These spatial variations in spectrum reflect corresponding differences in the electron-energy distributions at different points in the nebula. As expected, electrons with the highest energy are concentrated nearest the center, which is now universally recognized as the seat of acceleration.

B. Rotation Measure and Intrinsic Position Angle Distributions.

The polarization parameters of the integrated radiation from Taurus A are accurately known at several frequencies. There is consequently no ambiguity in the determination of the integrated rotation measure. Burn (1966) finds -25.6 rad m^{-2}. To resolve any $\pm n\pi$ ambiguities in position-angle difference between 1420 and 2880 MHz, we require that our calculated values be near this integrated value and that variations in rotation measure not be discontinous over dimensions comparable to the beamwidth. Since a difference of π rad between 1420 and 2880 MHz changes the rotation measure by 93 rad m^{-2}, we feel certain that the values presented in Table 3 are free from ambiguity.

The rotation-measure distribution varies extremely smoothly and over a surprisingly small range of values. A contribution to each of these rotation measures is made by the interstellar medium between the sun and the Crab Nebula. Manchester (1971)

has pointed out the similarities in rotation measure and dispersion measure of the two pulsars, 0531+21 and 0525+21, both believed associated with the Crab Nebula, and has argued convincingly that their rotation arises in the interstellar medium. We therefore adopt -4. rad m^{-2} as the interstellar rotation measure. By subtracting this value from those measured, we obtain the rotation measures produced internally in the Crab Nebula. These results are presented in Table 4.

Except near the eastern edge of the nebula, lines of constant rotation measure are parallel to the major axis. It seems unlikely that a gradient in the intervening interstellar medium would coincide with a principal axis of Taurus A[2], so that the variation in Table 4 probably represents changes in its internal magneto-ionic medium.

We have also calculated the distribution of intrinsic position angles using the rotation measures in Table 3 and the position angles measured at 2880 MHz. These results are shown in Fig. 4. Except in the northwest corner, the intrinsic angles vary little across the source. Over a central region of angular diameter ~ 2', the total scatter in angles is less than 10°. Over the main body of the nebula the intrinsic position angles are ~ 15° greater than the position angle of the major axis.

---

[2]Since the major axis of the Crab Nebula is closely parallel to the galactic equator (Münch 1958), this argument may be weakened somewhat.

C. Depolarization Ratio Distribution

The depolarization ratio (P_{1420}/P_{2380}) is computed over the face of the Crab and presented in Table 5. The percentage polarization at the lower frequency is nearly everywhere very close to half that at the higher. There is no obvious systematic spatial trend in the ratios. Coupled with the previously noted systematic variation in rotation measures, this indicates that depolarization and rotation are not strongly correlated. Since correlation would be expected in a uniform Faraday medium, we conclude that the magneto-ionic medium internal to the Crab Nebula has non-uniformities on a scale much smaller than our beamwidth (i.e., $<<0.5$ parsec).

IV. DISCUSSION

With our resolution of ~1 arcmin (corresponding to ~ 0.5 pc at a distance of 1.7 kpc), the overall impression of Taurus A is one of extraordinary large-scale uniformity in its structure, as revealed by the following evidence:

(a) The total brightness distribution is very smooth and simple (Figs. 2 and 3).

(b) The intrinsic polarization angles show little variation over most of the main body of the nebula (Fig. 4). This implies a uniform direction for $H_\perp$, the component of internal magnetic field normal to the line of sight.

(c) The rotation measures vary smoothly, slowly and only over a small range. (Table 3 or 4). This implies the product $n_e H_{||}$, where n_e is the density of thermal gas, is relatively constant.

(d) The depolarization ratios are nearly constant (Table 5), implying that the scale of irregularities and the energy density in turbulent magnetic fields changes little.

However, coexisting with this large-scale ordering of the Crab Nebula is a chaotic fine structure. This can be seen by:

(a) The prominent optical filaments (Woltjer 1958; Trimble 1968) reveal directly high density concentrations on a scale $\sim 10^{-2}$ pc.

(b) The optical continuum emission has a fine, fibrous structure with details at the limit of resolution ($\leq$ 1 arcsec (corresponding to $< 10^{-2}$ pc; Scargle 1969).

(c) Fine structure is seen in high resolution radio studies (Wilson 1971).

(d) The continuum radiation from optical to long radio wavelengths is strongly depolarized. Burn (1966) has explained this in terms of a spread in Faraday depths over several orders of magnitude. The available decimetric wavelength polarization distributions reveal that portions of the polarized emission radiate through gaps in a highly depolarizing screen (Downs and Thompson 1968; Wright 1970; present paper). The highest resolution radio polarization study (Conway 1971) reveals that this depolarizing screen has a scale < 7" (or $<$0.06 pc).

(e) The polarized radiation from the pulsar 0531+21, presumably located at the center of the nebula, apparently receives little or no Faraday rotation from the nebula (Manchester 1971). This is direct evidence for at least one hole in the magneto-plasma.

(f) The constant linear polarization of the optical continuum near the pulsar implies that the scale of the fine structure is less than 0.02 pc (Forman and Visvanathan 1971).

A. The Uniform Magnetic Field

Our measurements clearly refer primarily to the overall large-scale magnetic field. Using synchrotron theory (Ginzburg and Syrovatskii 1965), we can estimate the distribution of magnetic-field strengths. These are presented in Table 6. We have assumed that the Crab Nebula is a uniformly filled prolate spheroid (prolate vs. oblate case argued in, e.g., Shklovsky 1968, pp. 311, 312) with semi-major and semi-minor axes, which lie in the plane of the sky, of dimensions 1.61 and 1.25 pc, respectively, at a distance of 1.7 kpc (Minkowski 1971). We have also assumed equipartition between the energies of the magnetic field and of the relativistic electrons (see Shklovsky 1968, pp. 316-318 for arguments for ignoring protons), and have used the spectral index distribution from Table 2 and the brightness distribution at 1420 MHz (Fig. 2).

The field strengths in Table 6 represent the quantity $\sqrt{H_o^2+H_r^2}$, where H_o is a uniform field and H_r an isotropic random field, averaged along lines-of-sight through the nebula. This quantity decreases only slightly from ~ 2.5×10^{-4} G at the center to ~ 1.9×10^{-4} G near the edges.

We can also estimate the relative contributions of the random and uniform components of the field. The fractional polarization expected in a uniform magnetic field is $p(\alpha)=(3-3\alpha)/(5-3\alpha)$, where α is the spectral index. We find that $p(\alpha)$ varies from ~ 0.66 near the center of Taurus A to ~ 0.75 near the edges. However, even at the short wavelength of 1.55 cm the fractional polarization p_i reaches a maximum of only ~ 0.16 near the center and falls to less than half this value near the edges (Mayer and Hollinger 1968). The field obviously has a sizeable random component, therefore, which can be estimated from the relation (Burn 1966)

$$p_i=p(\alpha)\frac{H_o^2}{H_o^2+H_r^2} \quad .$$

Using the measurements at λ1.55 cm as indicative of the intrinsic degree of polarization p_i and our $p(\alpha)$ distribution, we estimate that the ratio $(H_r/H_o)^2$ varies from ~ 3 near the center to ~ 9 near the edges.

Knowing the distributions of both $(H_r/H_o)^2$ and $\sqrt{H_o^2+H_r^2}$, we can estimate the distributior of the strengths of the uniform

magnetic field. Referred to the peak of the polarization distribution (~0!5 southeast of our coordinate origin), the uniform field H_o, is

(a) ~ 1.2×10^{-4} G within the central 0!5;

(b) ~ 0.9×10^{-4} G at 1!0-1!5;

(c) ~ 0.6×10^{-4} G beyond 1!5.

The orientation of this uniform field can also be determined. The components normal to the line of sight are perpendicular to the intrinsic position angle vectors illustrated in Fig. 4. Since, except at the northwestern edge, nearly all of these vectors are within 10° of position angle 149°, the normal component, $H_{o\perp}$, is close to position angle 59° over the main body of the nebula, i.e., ~ 14° greater than the position angle of the minor axis. Further, from Table 4 we see that the rotation measure produced within the Crab Nebula is everywhere positive. Hence, the line-of-sight component of the uniform magnetic field, $H_{o||}$, is everywhere directed toward us. If we assume that $H_{o\perp}^2 \approx H_{o||}^2 \approx \frac{1}{2}H_o^2$, then the strength of $H_{o||}$ is 0.7 times the values of H_o listed above.

B. The Thermal Plasma.

From the known rotation measures in Taurus A (Table 4) we obtain directly the product $\langle n_e H_{o||} L \rangle$, where L is the pathlength through the nebula parallel to the line of sight. Assuming again that the nebula is a uniformly filled prolate spheroid with major axis in the plane of the sky, we can easily calculate L. We then have the product $\langle n_e H_{o||} \rangle$ of thermal electron density n_e

and line-of-sight uniform field $H_{o||}$. This product is displayed in Table 7. We can also estimate $\langle n_e H_{o||} \rangle$ from the depolarization produced by a uniform medium. The values calculated by this latter method are all larger. In other words, the measured depolarization exceeds that predicted from the rotation produced in a uniform slab. This reinforces the picture of coexisting uniform and finely structured media within the nebula: i.e., some radiation is depolarized by structure so fine that there is no net rotation.

We note that $\langle n_e H_{o||} \rangle$ is approximately constant along lines parallel to the major axis. Since we previously estimated that H_o decreased from center to edge, the electron density appears to increase near the edges. We estimate $n_e \sim 0.25$ cm^{-3} near the center of the nebula, increasing more or less smoothly in all radial directions to ~ 0.5 cm^{-3} at the periphery. Even larger values may be found at the northern boundary and at the extreme southwestern edge. Clearly our assumption of a uniformly dense medium was at best a crude approximation to reality. More likely, the thermal gas has a more shell-like distribution. This would support the ideas of Scargle (1969) and Rees (1971), who have argued that the pulsar activity in the Crab Nebula evacuates the thermal gas from the central region.

V. SUMMARY

From our investigations of the Crab Nebula we find that:

(1) The spectrum of the radiation is flattest at the center and progressively steepens in all outward directions.

(2) The magnetic field strength is ~ 2.5×10^{-4} G at the center and decreases to 75-80 per cent of this maximum value near the periphery.

(3) There is structure on a scale much less than our resolution ($<<0.5$ pc) co-mixed with a uniform large-scale medium.

(4) The strength of the small-scale random component of the magnetic field is ~ 1.8 times that of the uniform component near the center, changing to ≥ 3 times near the periphery.

(5) Throughout most of the nebula the projection of the uniform magnetic field onto the plane of the sky is near position angle 60°; there is also a component out of the plane of the sky toward us.

(6) The central region of the nebula has a relatively less dense thermal plasma than the periphery.

ACKNOWLEDGEMENTS

We wish to thank the members of the Owens Valley Staff and observers who have greatly assisted the collection and calibration of the data. We further wish to thank D. H. Rogstad for his assistance and discussion of inversion techniques and the members of the Kapteyn Laboratory, Groningen, Netherlands for their encouragement and the use of their facilities. We benefited greatly from discussions with M. C. H. Wright. Research at the Owens Valley Radio Observatory is supported by the Office of Naval Research under Contract N00014-67-A-0094-0019 and by the National Science Foundation under Grant GP30400-X.

REFERENCES

Branson, N.J.B.A. 1967, Nature 213, 1211.

Braun, L. D., and Yen, J. L. 1968, Ap. J. (Letters) 153, L123.

Burn, B. J. 1966, M.N.R.A.S. 133, 67.

Conway, R. G. 1971, Radio polarization of the Crab Nebula in The Crab Nebula, Eds. R. D. Davies and F. G. Smith, D. Reidel Publishing Co., Dordrecht, Holland, p. 292.

Davies, R. D., Gardner, F. F., Hazard, C., and Mackey, M. B. 1966, Australian J. Phys. 19, 409.

Downs, G. S., and Thompson, A. R. 1968, Ap. J. (Letters) 152, L65.

Forman, W., and Visvanathan, N. 1971, Nature 229, 39.

Ginzburg, V. L., and Syrovatskii, S. I. 1965, Ann. Rev. Astron. and Astrophys. 3, 297.

Hogg, D. E., Macdonald, G. H., Conway, R. G., and Wade, C. M. 1969, A. J. 74, 1206.

Johnston, K. J., and Hobbs, R. W. 1969, Ap. J. 158, 145.

Manchester, R. N. 1971, Nature Phys. Sci. 231, 189.

Mayer, C. H., and Hollinger, J. P. 1968, Ap. J. 151, 53.

Milne, D. K. 1971, Radio emission from supernova remnants in The Crab Nebula, Eds. R. D. Davies and F. G. Smith, D. Reidel Publishing Co., Dordrecht, Holland, p. 248.

Minkowski R. 1971, Comments on supernova remnants and ancient novae, ibid, p. 241.

Münch, G. 1958, Rev. Mod. Phys. 30, 1042.

Rees, M. J. 1971, Nature Phys. Sci. 230, 55.

Rogstad, D. H., and Shostak, G. S. 1971, Astron. and Astrophys. 13, 99.

Scargle, J. D. 1969, Ap. J. 156, 401.

Seielstad, G. A., and Weiler, K. W. 1968, Ap. J. 154, 817.

Shklovsky, I. S. 1968, Supernovae. John Wiley & Sons Ltd., London.

Trimble, V. 1968, A. J. 73, 535.

Weiler, K. W., and Seielstad, G. A. 1971, Ap. J. 163, 455, Paper I.

Wilson, A. S. 1971, High resolution maps of the Crab Nebula at 2700 MHz and 5000 MHz in The Crab Nebula, Eds. R. D. Davies and F. G. Smith, D. Reidel Publishing Co., Dordrecht, Holland, p. 68.

Woltjer, L. 1957, B.A.N. 13, 301.

_____ 1958, ibid. 14, 39.

Wright, M. C. H. 1970, M.N.R.A.S. 150, 271.

TABLE 1

Taurus A Error Estimates

Stokes Parameter	Error	
	1420 MHz (f.u. arcmin^{-2})	2880 MHz (f.u. arcmin^{-2})
I	4.5×10^{0}	5.7×10^{0}
Q	1.8×10^{-1}	1.1×10^{-1}
U	6.0×10^{-2}	5.1×10^{-1}

TABLE 2

Spectral Index Distribution ($I_\nu \sim \nu^{+\alpha}$)

Minor Axis (arcmin) \ Major Axis (arcmin)	3.'0	2.'5	2.'0	1.'5	1.'0	0.'5	0.'0	0.'5	1.'0	1.'5	2.'0	2.'5	3.'0
1.'5		-1.00	-0.69	-0.57	-0.58	-0.65	-0.81	-0.83	-0.99	-1.61			
1.'0	-1.02	-0.79	-0.58	-0.50	-0.44	-0.44	-0.49	-0.47	-0.56	-0.69	-0.72	-1.09	
0.'5	-0.89	-0.6[illegible]	-0.55	-0.49	-0.38	-0.37	-0.35	-0.34	-0.45	-0.51	-0.52	-0.69	
0.'0	-0.96	-0.67	-0.60	-0.54	-0.42	-0.42	-0.36	-0.36	-0.42	-0.47	-0.50	-0.60	-0.75
0.'5	-1.05	-0.66	-0.58	-0.53	-0.45	-0.46	-0.36	-0.33	-0.40	-0.42	-0.47	-0.53	-0.69
1.'0		-0.64	-0.54	-0.48	-0.44	-0.44	-0.36	-0.35	-0.43	-0.41	-0.58	-0.59	
1.'5			-0.64	-0.55	-0.50	-0.51	-0.46	-0.48	-0.54	-0.54	-0.70	-0.99	
2.'0				-0.67	-0.61	-0.60	-0.53	-0.54	-0.70	-0.91			
2.'5						-0.34	-0.47	-0.65					

TABLE 3

Rotation Measure Distribution (rad m^{-2})

Minor Axis (arcmin) \ Major Axis (arcmin)	2.'0	1.'5	1.'0	0.'5	0.'0	0.'5	1.'0	1.'5	2.'0	2.'5
1.'5		-28	-27	-25						
1.'0		-28	-26	-25	-24	-22	-21	-22	-28	
0.'5	-30	-26	-25	-24	-23	-23	-23	-22	-25	-28
0.'0	-26	-24	-23	-23	-23	-23	-23			-27
0.'5		-21	-21	-21	-21	-21	-21			
1.'0		-18	-19	-19	-20	-19				
1.'5				-16	-18	-19				
2.'0					-16					

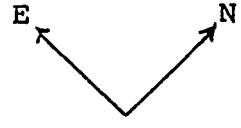

TABLE 4

Internal Rotation Measure Distribution (rad m^{-2})

Minor Axis (arcmin) \ Major Axis (arcmin)	2.'0	1.'5	1.'0	0.'5	0.'0	0.'5	1.'0	1.'5	2.'0	2.'5
1.'5		14	15	17						
1.'0		14	16	17	18	20	21	20	14	
0.'5	12	16	17	18	19	19	19	20	17	14
0.'0	16	18	19	19	19	19	19			15
0.'5		21	21	21	21	21	21			
1.'0		24	23	23	22	23				
1.'5				26	24	23				
2.'0					26					

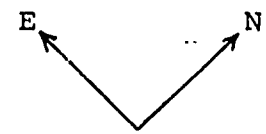

TABLE 5

Depolarization Ratio Distribution (P_{1420}/P_{2880})

Minor Axis (arcmin) \ Major Axis (arcmin)	2.0	1.5	1.0	0.5	0.0	0.5	1.0	1.5	2.0	2.5
1.5		0.50	0.48	0.47						
1.0		0.52	0.47	0.44	0.43	0.48	0.50	0.44	0.41	
0.5	0.81	0.52	0.45	0.43	0.44	0.48	0.57	0.58	0.47	0.55
0.0	0.80	0.51	0.44	0.41	0.44	0.46	0.54			0.62
0.5		0.51	0.41	0.36	0.41	0.47	0.54			
1.0		0.49	0.40	0.37	0.46	0.54				
1.5				0.51	0.58	0.63				
2.0					0.66					

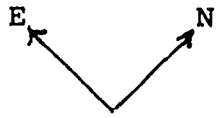

TABLE 6

Magnetic Field Strength Distribution (10^{-4} Gauss)

Minor Axis (arcmin) \ Major Axis (arcmin)	3.0	2.5	2.0	1.5	1.0	0.5	0.0	0.5	1.0	1.5	2.0	2.5	3.0
1.5		3.2	1.9	1.8	1.9	2.0	2.3	2.3	2.7				
1.0		2.4	2.0	2.0	2.1	2.1	2.2	2.1	2.1	2.1	2.0	2.7	
0.5	2.8	2.2	2.1	2.1	2.2	2.3	2.4	2.4	2.3	2.2	2.1	2.1	
0.0	2.8	2.1	2.1	2.2	2.3	2.4	2.4	2.4	2.3	2.3	2.2	2.0	2.0
0.5	3.0	2.1	2.1	2.2	2.3	2.4	2.5	2.5	2.3	2.2	2.2	2.0	2.0
1.0		1.9	2.0	2.2	2.2	2.3	2.4	2.4	2.2	2.2	2.1	2.0	
1.5			1.9	2.0	2.1	2.2	2.2	2.1	2.1	2.0	2.1		
2.0				1.9	1.9	2.0	2.0	2.0	2.1	2.7			
2.5							2.5						

E

N

TABLE 7

Distribution of $\langle n_e H_{o||} \rangle$ (10^{-5} cm^{-3} Gauss)

Minor Axis (arcmin) \ Major Axis (arcmin)	2.'0	1.'5	1.'0	0.'5	0.'0	0.'5	1.'0	1.'5	2.'0	2.'5
1.'5		2.1	2.1	2.1						
1.'0		1.7	1.9	1.8	1.9	2.2	2.4	2.4	2.1	
0.'5	1.6	1.8	1.9	1.9	1.9	1.9	1.9	2.4	2.2	2.3
0.'0	2.0	2.0	2.0	2.0	2.0	2.0	1.9			2.3
0.'5		2.4	2.3	2.2	2.1	2.2	2.3			
1.'0		3.0	2.7	2.5	2.5	2.5				
1.'5				3.2	3.0	2.9				
2.'0					4.3					

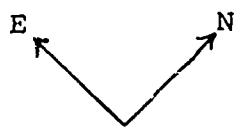

FIGURE CAPTIONS

Fig. 1. Portion of the Fourier (u, v)-plane covered at the declination of Taurus A.

(a) 1420 MHz; 0-1600 feet E/W and N/S in basic increments of 200 feet; 100 feet spacing included E/W; 1000 and 1200 foot spacings missing N/S. Crosses mark every hour of hour angle; scales in thousands (10^3) of wavelengths.

(b) 2880 MHz; 0-800 feet E/W in increments of 100 feet; 0-800 feet N/S in increments of 200 feet; 500 foot spacing missing E/W. Crosses mark every hour of hour angle; scales in thousands (10^3) of wavelengths.

Fig. 2. Distributions of total and linearly polarized radiation over Taurus A at 1420 MHz. North at top and east on left. Origin at $\alpha_{1950}=05^h31^m31^s.20$, $\delta_{1950}=21°59'17''.0$.

(a) total radiation; half-power beamwidth shown in upper left-hand corner; 10=76.8 x 10^{-26}W m^{-2} Hz^{-1} $arcmin^{-2}$.

(b) polarized radiation; 20 per cent contour darkened; 10=2.3x10^{-26}W m^{-2} Hz^{-1} arc min^{-2}.

(c) position angle of the polarization; orientation of the line gives position of the electric vector; degree of linear polarization indicated by line length; line length appropriate for 5 per cent polarization shown in lower left-hand corner.

Fig. 3. Taurus A; 2880 MHz (see caption to Fig. 2).

(a) total radiation; 10=56.2 x 10^{-26}W m^{-2} Hz^{-1} $arcmin^{-2}$.

(b) polarized radiation; 20 per cent contour darkened; 10=4.3 x 10^{-26}W m^{-2} Hz^{-1} $arcmin^{-2}$.

(c) electric vectors; line length appropriate for 10 per cent polarization shown in lower left-hand corner.

Fig. 4. Intrinsic position angle of the electric vector for Taurus A. Solid line, delimiting 1420 MHz contour; dashed line delimiting 2880 MHz contour. Line length has no significance.

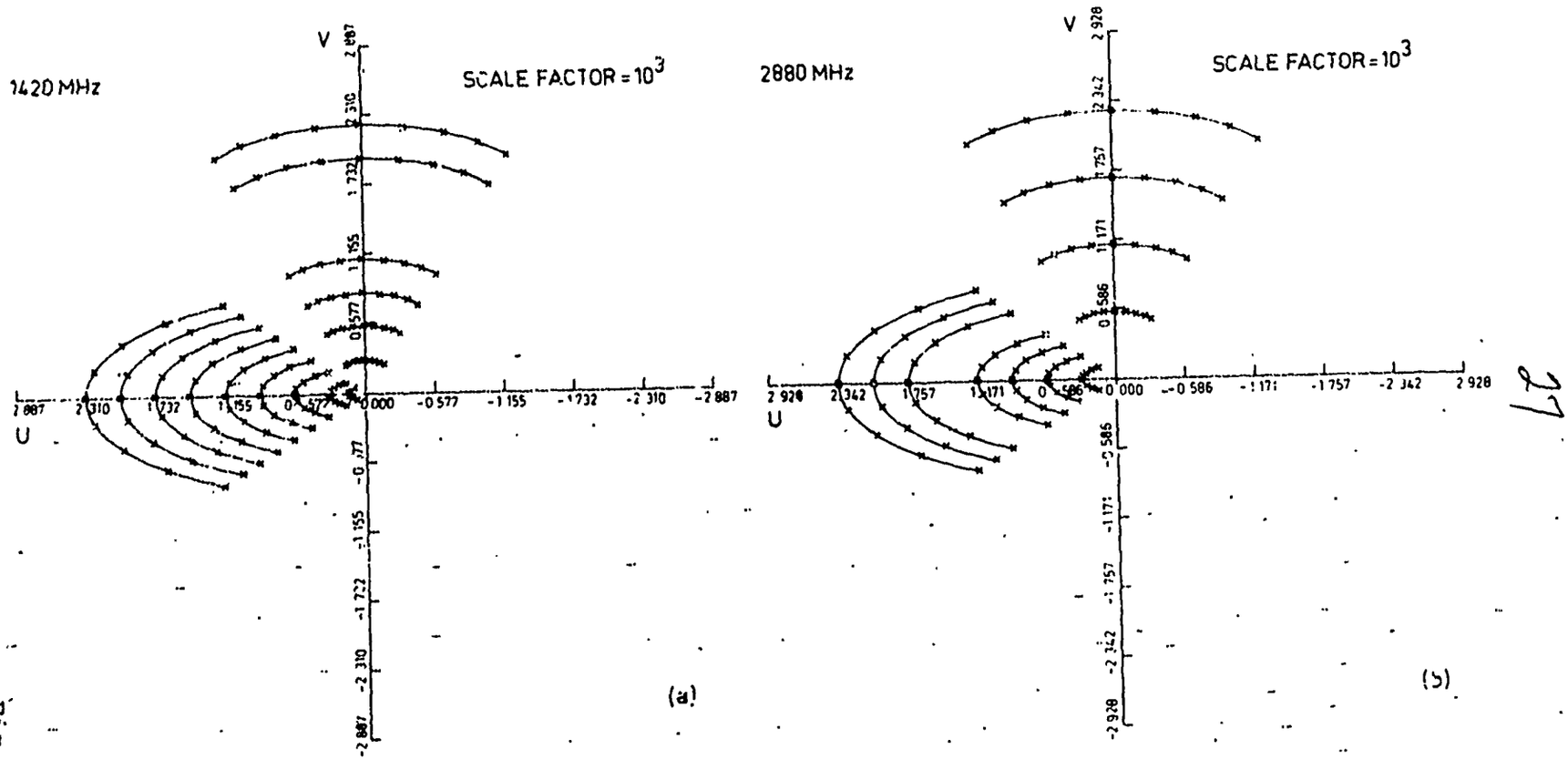
1420 MHz
SCALE FACTOR = 10^3
V
U
2 887
2 310
1 732
1 155
0 577
0 000
-0 577
-1 155
-1 732
-2 310
-2 887
(a)
2880 MHz
SCALE FACTOR = 10^3
V
U
2 928
2 342
1 757
1 171
0 586
0 000
-0 586
-1 171
-1 757
-2 342
-2 928
(b)

Fig. 1

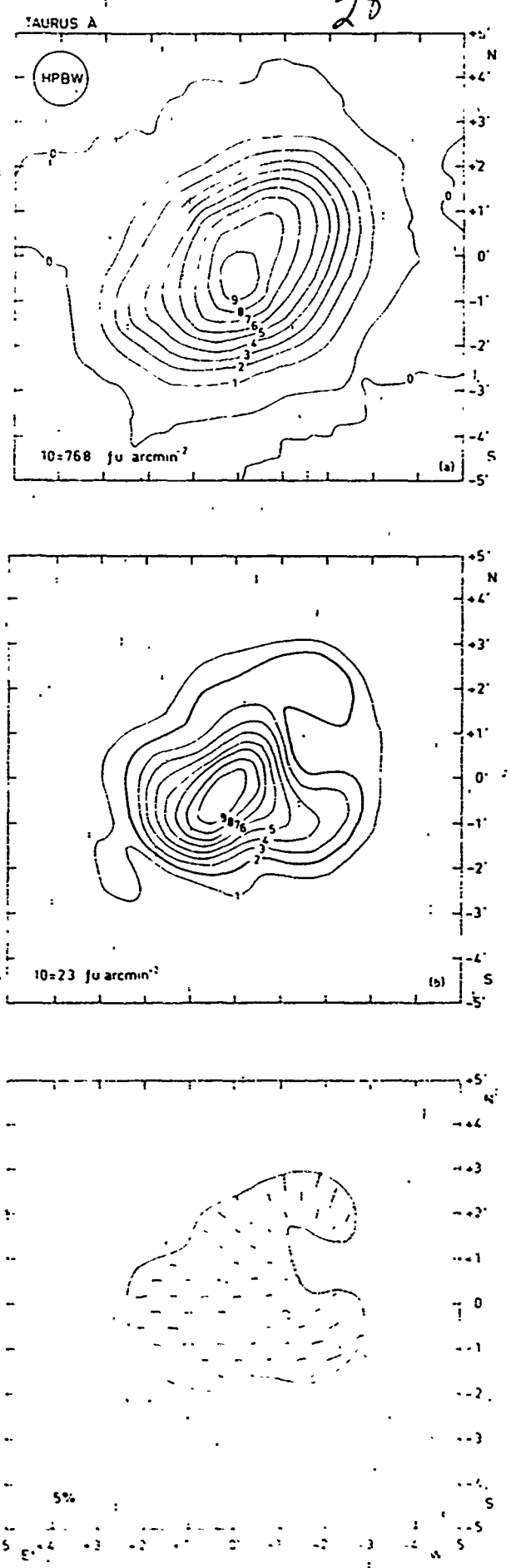

Fig. 2

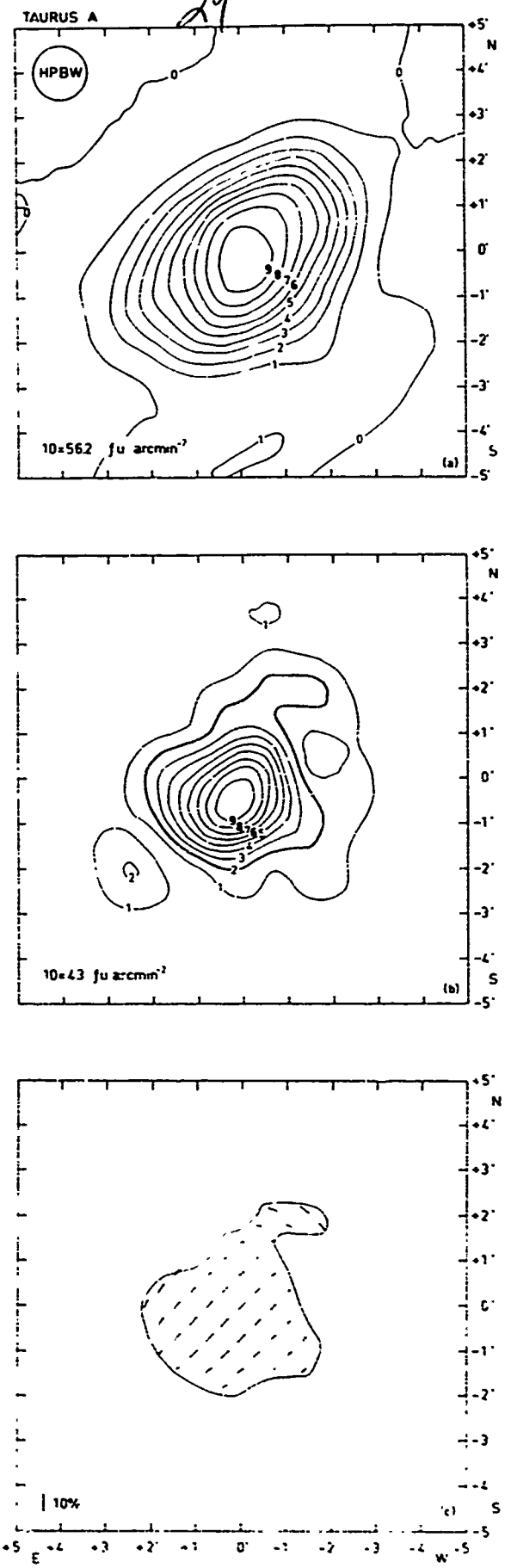

Fig. 3

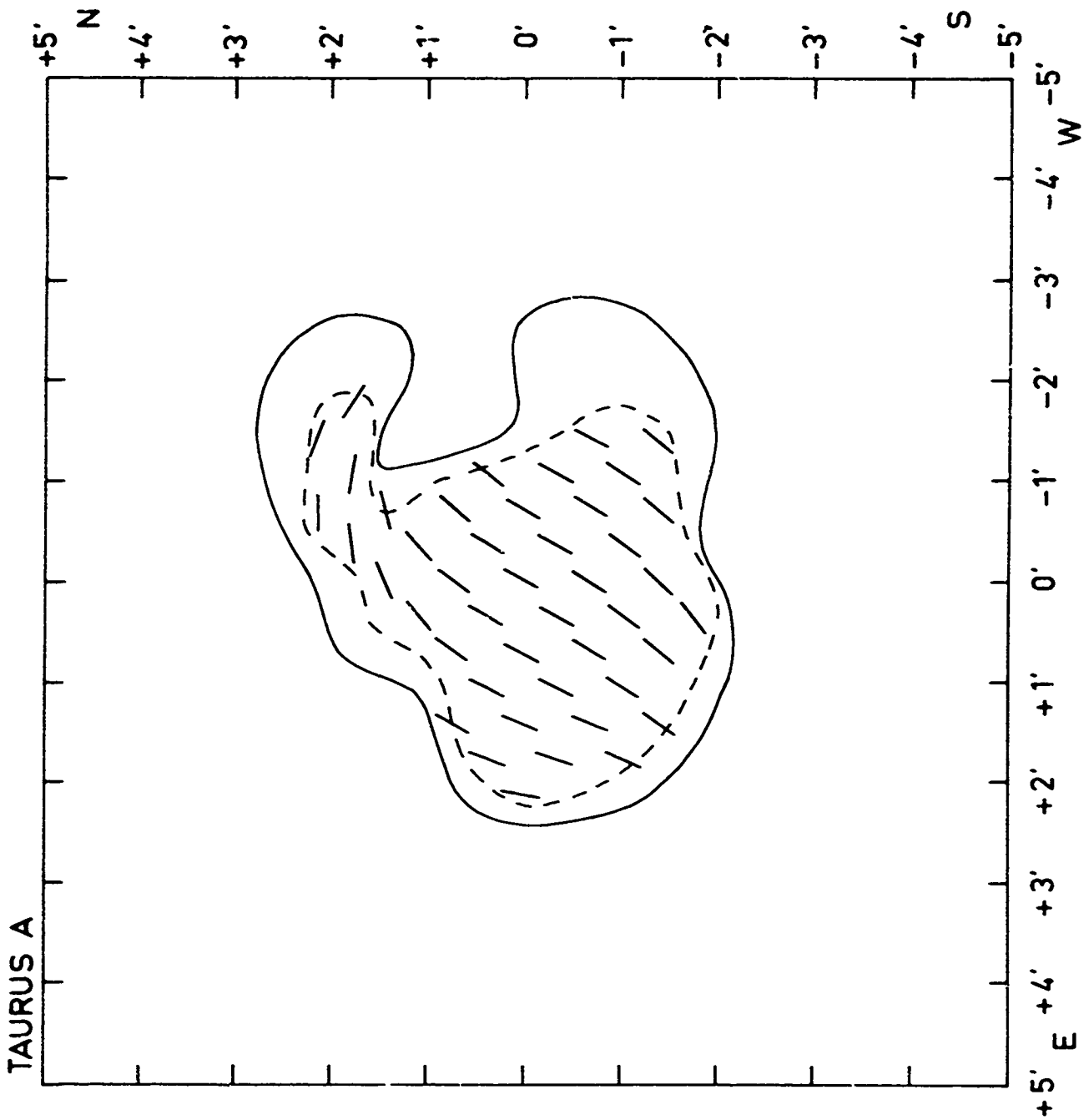

Fig. 4